RSC Advances

PAPER

View Article Online
View Journal | View Issue

Cite this: *RSC Adv.*, 2017, **7**, 17164

Enhanced temperature stability and exceptionally high electrical contrast of selenium substituted $Ge_2Sb_2Te_5$ phase change materials†

Christine Koch,[a] Anna-Lena Hansen,[a] Torben Dankwort,[b] Gerrit Schienke,[a] Melf Paulsen,[a] Dominik Meyer,[c] Martin Wimmer,[c] Matthias Wuttig,[c] Lorenz Kienle[b] and Wolfgang Bensch*[a]

Received 25th January 2017
Accepted 3rd March 2017

DOI: 10.1039/c7ra01140g

rsc.li/rsc-advances

$Ge_2Sb_2Te_4Se$ (I) and $Ge_2Sb_2Te_2Se_3$ (II) thin films were synthesized and compared to the pure telluride $Ge_2Sb_2Te_5$. *In situ* X-ray diffraction (XRD) and *in situ* transmission electron microscopy (TEM) investigations revealed a remarkably increased stability of the as-deposited amorphous phase. The transition temperature (beginning transition) determined with *in situ* XRD increases from 135 °C for the pure telluride to 165 °C for (I) and to 225 °C for (II). An identical trend for the transition temperatures (transition complete) was observed by sheet resistance measurements with values of 153, 190 and 243 °C, respectively. Optical properties determined with Fourier-transform-infrared (FTIR) spectroscopy and variable incident angle spectroscopic ellipsometry (VASE) exhibit a significant energy-dependent behavior of the dielectric functions. Major changes of the maxima and intensities of the extinction coefficients and the indices of refraction are observed with increasing Se content. These results are in agreement with the results obtained by Rietveld refinement and TEM. The incorporation of Se into the structure of the metastable cubic phase causes small distortions, leading to a phase transition. Electrical sheet resistance measurements reveal an exceptionally large electrical contrast between the amorphous and crystalline phases, which is increased by a factor of 100 for compound (II) compared to established phase change materials.

Introduction

Today, data storage is of particular technological importance. For the last few thousands of years information was stored, starting with drawings and paintings, improving with letters and books, up to computers containing data storage devices. Because of the increasing amount of data, larger and faster memory devices of smaller sizes are required. In case of optical data storage, long-term stability, repeatability and reliability need to be improved, as well as the data density and the opto-electronic contrast. Additionally, the costs of the materials should be as low as possible and easy fabrication is required.[1,2] These criteria are met for phase change materials (PCM).[3,4] Most phase change materials are based on the pseudo-binary section of the binary compounds GeTe and Sb_2Te_3 yielding compositions like $(GeTe)_m(Sb_2Te_3)_n$. Another very interesting composition is AIST, a combination of the elements Ag, In, Sb and Te.[5] These materials can rapidly and reversibly be switched between an amorphous and a crystalline state applying a laser with short pulses and high powers. The amorphous and crystalline states have remarkably different optical properties that are easily detected by the laser. For erasing the bit (recrystallization) a longer lasting pulse with lower intensity is used.

During the last decades three different generations of optical data storage devices were developed: compact discs (CD, using a laser wavelength of 830 nm), digital versatile discs (DVDs, 650 nm) and Blu-ray™ discs (BD, 405 nm). Further decreasing the laser wavelength has been proven difficult due to several challenges including the lack of suitable laser diodes, but also a decreasing contrast of phase change materials at shorter wavelengths. Further, phase change materials have been studied for their application potential in non-volatile electronic memories. They can be rapidly and reversibly switched if a low voltage pulse is applied and they have already proven excellent scaling potential. Yet, there are still a number of issues to be addressed in order to understand the full potential of these novel memories. Two questions are of particular interest for applications at elevated temperatures, such as automotive applications, namely: at which temperature will the amorphous phase crystallize and how high is the resistance of the

[a]Institute for Inorganic Chemistry, University of Kiel, Max-Eyth-Str. 2, 24118 Kiel, Germany. E-mail: wbensch@ac.uni-kiel.de
[b]Institute for Materials Science, University of Kiel, Kaiserstr. 2, 24143 Kiel, Germany
[c]Institute of Physics, RWTH Aachen University, Sommerfeldstr. 14, 52056 Aachen, Germany

† Electronic supplementary information (ESI) available. See DOI: 10.1039/c7ra01140g

amorphous phase. While the stability of the amorphous phase is crucial for applications at elevated temperatures, a high resistance of the amorphous state could facilitate realizing a multi-level memory.[6,7]

In recent years, two major research approaches were followed for further improvement of phase change materials. One research direction is focused on unravelling the atomistic origin of the high switching speeds, the aging of the amorphous state and the pronounced property contrast between the two states.[8] The structure of the crystalline phase is in most cases a distorted rock salt structure with different vacancy concentrations in the cation sublattice depending on the chemical composition.[9–12] From a chemical point of view it is not easy to explain that Ge and Sb in $Ge_2Sb_2Te_5$ each are in an octahedral environment of Te^{2-} anions. One approach to rationalize this bonding situation is called resonant bonding where sharing of electrons (covalent bonds) leads to stabilization of highly symmetric coordination. To avoid confusion with the term resonant bonding used in organic chemistry to describe the bonding situation in high symmetric materials like benzene or graphite, resonant bonding in PCMs has a different meaning.[6,13–15]

The local atomic structures of the different phases were also intensively investigated.[16–22] Despite many efforts, the short-range coordination of the different atoms in the amorphous structure are still under debate in literature.[16,23–26] These problems demonstrate that it is not trivial to investigate and understand the reactions on atomic scale of the phase change, yet being the essential issue for designing new materials. Hence, in a second approach, scientists have tried to identify new compounds, which also exhibit the characteristic properties of phase change materials.

So far, many studies have focused on $Ge_2Sb_2Te_5$.[27–30] Due to its excellent properties it was used as the DVD-RW material. Other well investigated compounds are $GeCu_2Te_3$ (ref. 31–33) and $Ge_8Sb_2Te_{11}$ being the active material in BD-RW discs or binaries such as $Ge_{15}Sb_{85}$,[34] GeTe[35] and GaSb,[36–39] respectively. Several studies deal with the substitution or doping of established phase change materials.[40–45] Samples with compositions $(Ge_2Sb_2Te_5)_{1-x}Se_x$ (x = 0–0.5) were recently investigated, showing a significantly different crystallization behavior. For $x \geq 0.1$ the stable hexagonal structure is directly formed at $T \geq 150$ °C, while the metastable cubic phase could only be observed for $x \leq 0.02$. With increasing Se content the optical band gap becomes larger. In addition, the resistance, threshold voltage and thermal stability increased with x. For the Se substituted materials a relatively low crystallinity of the crystalline phases was observed.[46,47] Compared to $Ge_2Sb_2Te_5$ no significant improvement in properties could be observed and a relationship of properties with structural changes could not be established.

In our ongoing work the impact of the substitution of Te in $Ge_2Sb_2Te_5$ by Se on the material properties was investigated. The substitution in the anion substructure of the metastable cubic rock salt structure should lead to local distortions, a decreased metallic character and a larger electronegativity difference, which increases at the same time hybridization and ionicity. As a result of these pronounced changes of the physico-chemical properties significant alterations of the optical and electrical behavior are expected. Additionally, the bond strength and therefore the phase change transition temperatures should be altered. The final goal of the present investigation is to establish a relationship between the change in the chemical bonding by chemical substitution of Te by Se and the resulting properties. The results of these experiments and the observed trends concerning the opto-electronic properties and the bonding characteristics are reported.

Experimental section

Thin film samples of $Ge_2Sb_2Te_5$ and $Ge_2Sb_2Te_4Se$ (I) were prepared by DC magnetron sputtering using stoichiometric targets (Umicore, 99.99%) bonded to water cooled copper plates. The base pressure in the sputter chamber was $<2 \times 10^{-6}$ mbar, the argon current was fixed at 20 sccm for all deposition runs. $Ge_2Sb_2Te_5$ was deposited by using a single target of 10 cm diameter at 20 W. (I) was prepared *via* co-sputtering of $GeSb_2Te_4$ (5 cm diameter) at 30 W and GeSe (10 cm diameter) at 25 W.

All substrates had a size of 2 × 2 cm. Thin film samples of ~700 nm thickness were prepared on (1 0 0) silicon single crystal substrates, glass substrates, glass substrates with previously sputtered chromium contacts in the corners (for electrical measurements) and silicon substrates coated with ~200 nm aluminum layers (for optical measurements). Thin samples of ~35 nm were deposited on nickel TEM-grids, coated with a thin amorphous carbon layer. The deposition times of the thick and thin films were 3688 s (~700 nm) and 132 s (~35 nm) for $Ge_2Sb_2Te_5$ and 2000 s (~700 nm) and 75 s (~35 nm) for $Ge_2Sb_2Te_4Se$ (I).

$Ge_2Sb_2Te_2Se_3$ (II) was prepared by thermal co-evaporation of single elements in an ultra-high vacuum chamber (Omicron NanoTechnology), using single element Knudsen cells containing the utilized elements (Chempur 99.999%) at different temperatures, listed in Table 1. The base pressure in the chamber was $p < 1 \times 10^{-8}$ mbar. A beam flux monitor was used to ensure stable evaporation rates.

It should be noted that it is very important to find a reliable method to determine the compositions, because the signals of the elements partly overlap in most common analytic techniques due to their similar electronic structure. We found that electron probe micro-analysis (EPMA) is the most promising and precise method for investigating the X-ray emission L-series of the elements, using an acceleration voltage of 10, 16 and 22 kV. The EPMA measurements were taken with a Cameca SX 100, yielding composition values close to the required stoichiometries. A Bruker DektaktXT profilometer was used to determine the film thicknesses.

Table 1 Deposition temperatures of the single elements for preparing $Ge_2Sb_2Te_2Se_3$

Element	Germanium	Antimony	Tellurium	Selenium
Temperature/°C	1100	348	233	140
Deposition time	9 h (700 nm); 30 min (~35 nm)			

X-Ray diffraction (XRD) was performed in θ–θ geometry using an X'Pert Pro MPD diffractometer (PANalytical; Cu K$\alpha_{1,2}$ radiation), equipped with a Göbel mirror and a PIXcel detector. Temperature dependent *in situ* diffraction was performed in an Anton Paar HTK 1200N high temperature chamber in helium (99.999%) atmosphere to prevent oxidation of the samples. The temperature was increased stepwise with a heating rate of 5 K min^{-1} from 28 °C up to 360 °C. The patterns were collected within one hour over a range of 15–65° 2θ at constant temperature. The scans for the Rietveld refinements were performed on a flat stage using the same setup in a range of 10–100° 2θ (step size 0.05°).

Rietveld refinements were carried out using the Program TOPAS Academic (Version 6).[48] In order to calculate crystallite sizes the fundamental parameter approach was employed.[49,50] To refine the anisotropic peak broadening caused by strain we used a spherical harmonics to calculate the Lorentz width as a function of tan(θ). To correct texture effects, which are typical for thin film analysis, a spherical harmonics was employed.

In situ heating TEM experiments were performed by a FEI Tecnai F30 G^2 using a GATAN double tilt heating holder 652. The heating rate was set to 10 K min^{-1}. After the desired temperature was reached, a holding time was utilized until minimum sample drift and temperature equilibrium were achieved. Subsequently electron diffraction patterns were recorded at the rim of the grid, close to the measuring and heating device to ensure high accuracy of the actual temperature of the sample. For HRTEM and bright field imaging the heating was interrupted to ensure no sample drift.

To investigate the optical properties FTIR and ellipsometry measurements were done. FTIR spectra have been collected using a Bruker IFS 66v/s with a resolution of 0.12 meV. To exclude drift effects the samples and a gold reference were measured alternately. The measured spectra were renormalized by a gold reference to obtain the final spectrum. For ellipsometry measurements a J. A. Woollam M-2000UI equipped with deuterium and halogen lamps as light sources was used. The incidence angles were 65°, 70° and 75°. The examined energy ranges were 0.05–1 eV for FTIR and 0.7–5.2 eV for ellipsometry. All measurements were performed with the as-deposited amorphous samples as well as the metastable crystalline samples each on aluminum coated silicon substrates at room temperature. These substrates were prepared by sputter deposition of an aluminum target with the same process as described above. The values for the dielectric constants as well as the index of refraction n and the extinction coefficient k were obtained by fitting the spectra using SCOUT software.[51] Therefore the same assumptions as in ref. 42 were made.

Sheet resistance measurements were performed using a four-point-probe setup according to van-der-Pauw[52–55] with argon (99.996%) as protective gas. ~700 nm thick samples on glass substrates with chromium contacts in each corner were heated with a heating rate of 5 K min^{-1} up to 360 °C. This temperature was held constant for 30 min and then the samples were cooled down to room temperature. Because of the large density change of up to 10% between the amorphous and crystalline phases which unfortunately cannot be investigated and corrected during the resistivity measurements the resistance of the films instead of the resistivity was investigated.

Results and discussion

Structural characterization by *in situ* XRD and TEM heating experiments

In situ X-ray diffraction and TEM investigations were performed to independently investigate the structure and crystallization of the films. Both methods confirm that all as deposited films are amorphous. Thin films of $Ge_2Sb_2Te_5$ crystallize in the metastable cubic ($Fm\bar{3}m$) and the stable primitive trigonal ($P\bar{3}m1$) phase, respectively.[56]

For the accurate determination of the transition temperatures the intensities of the (002) reflection of the cubic and the (103) reflection of the primitive trigonal phase were analyzed as function of temperature (Fig. 1 and 2). While the 1st transition temperature increases with higher selenium content the temperature of the 2nd transition to the thermodynamically stable phase remains quite constant at around 270–290 °C. All three samples are stable until 360 °C.

In situ TEM heating experiments were performed by monitoring the formation of diffraction spots in the Selected Area Electron Diffraction (SAED) pattern. A representative temperature resolved image of this process is depicted in Fig. 3 for $Ge_2Sb_2Te_2Se_3$. Crystallization started at 132 °C, 160 °C and 222 °C, for $Ge_2Sb_2Te_5$, $Ge_2Sb_2Te_4Se$ and $Ge_2Sb_2Te_2Se_3$, respectively (for details see Fig. S1 and S2†). Further, diffuse streaks in the ED pattern were found for $Ge_2Sb_2Te_2Se_3$ after reaching the temperature of 250 °C (Fig. 3). These diffuse streaks indicate the formation of planar defects which can be attributed to vacancy layers forming along the (111) planes with respect to the cubic symmetry.[9,57,58]

A comparison of the transformation temperatures determined by *in situ* XRD and *in situ* TEM are displayed in Table 2. Phase change temperatures exhibit convincing agreement and confirm the monotonous increase of the crystallization temperature with increasing Se content. The values of $Ge_2Sb_2Te_5$ correspond well to those reported in literature.[27,59,60] Further, the substitution of Te by Se leads to a significant stabilization of the amorphous phase and therefore to a stabilization of amorphous areas/bits in data storage applications. Similar effects were also observed for other Ge–Sb–Te phases upon Se substitution.[40]

Bright field (BF) and high resolution TEM (HRTEM) images of $Ge_2Sb_2Te_5$ after the heating process revealed a mixture of larger grains with 100 nm size and nanocrystals marked by red and blue arrows in Fig. 4a, respectively. In comparison Se substituted films showed significantly smaller crystallites, *cf.* Fig. 4b and c displaying exclusively nanosized crystallites for (I) and (II).

Room temperature XRD data was analyzed *via* Rietveld refinement of the metastable phase revealing the same tendency for the crystallite size as found in TEM measurements (see Table 3 and Fig. 5).

The refinement indicated a symmetry reduction due to the incorporation of Se and a resulting distortion of the lattice

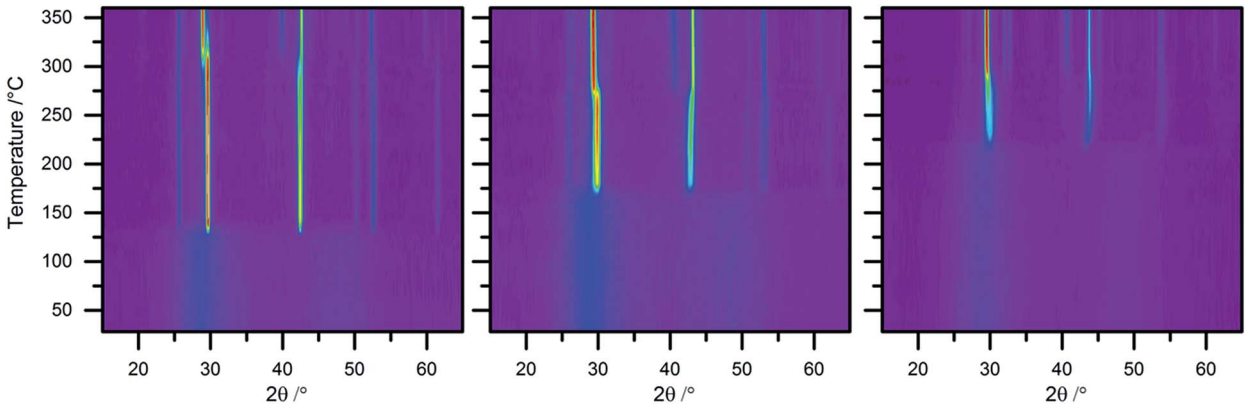

Fig. 1 *In situ* XRD patterns of $Ge_2Sb_2Te_5$ (left), $Ge_2Sb_2Te_4Se$ (middle) and $Ge_2Sb_2Te_2Se_3$ (right). Transitions from amorphous to cubic (rhombohedral trigonal) to primitive trigonal phases are seen by the appearance and disappearance of reflections.

along [111]. The latter caused a shift of the (220) reflection and anisotropic strain broadening. In the diffraction pattern of $Ge_2Sb_2Te_2Se_3$ we finally observe a splitting of the cubic (111) reflection, typically for a reduced symmetry (inset of Fig. 5).

To account for the lower symmetry, the cubic cell was transformed into the trigonal subgroup $R\bar{3}m$ (hexagonal axes). Due to the small crystallite size and the additional strain broadening, a splitting of the (220) reflection could not be observed, but its shift to lower scattering angle clearly represents a reduction of cubic symmetry even if the distortion itself is small. When compared to the transformed undistorted cell, it is apparent that the deviation from the cubic aristotype is more pronounced for the higher Se content. Calculated *d*-values based on the Rietveld refinements match closely with measured *d*-values of ED patterns (Tables S1–S3†).

Optical properties

It was already pointed out that resonant bonding is an indispensable property for high optical contrast of PCMs. As a result of the distortion in the substituted samples the octahedral environment of the atoms is distorted which leads to a misalignment of the p-orbitals and therefore to a significant reduction of the resonant bonding in the metastable phase. This corresponds well with the so called "treasure map" for PCM (Fig. 6).[14]

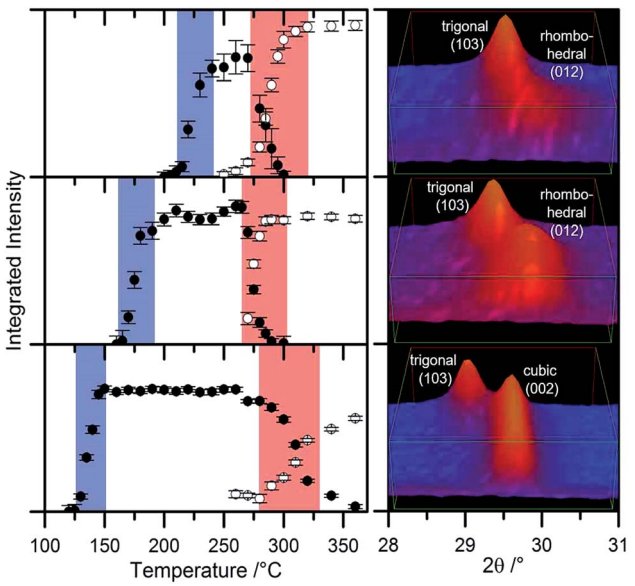

Fig. 2 Left: Determination of the phase change temperatures of $Ge_2Sb_2Te_5$ bottom, (I) middle and (II) top obtained by comparison of the diffraction intensities of the cubic (002)/rhombohedral (012) reflections (black circles) and primitive trigonal (103) reflection (white circles). Blue: phase change from amorphous to cubic (rhombohedral). Red: phase change from cubic to primitive trigonal. Right: Observation of the temperature induced phase transitions by evaluation of the reflection intensities.

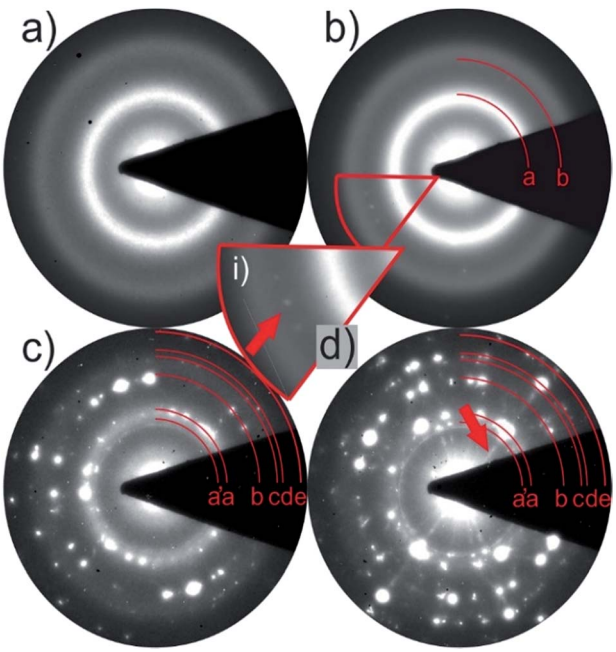

Fig. 3 SAED pattern of $Ge_2Sb_2Te_2Se_3$ (a) at room temperature; (b) crystallization starts at 222 °C (diffraction spots marked with red arrow); (c) growth of larger grains at 240 °C; (d) C diffuse streaks along [111] (rhombohedral cell) indicate formation of vacancy layers at 250°. Measured *d*-values fit to the calculated data can be found in Table S3.†

Table 2 Phase change temperatures of the synthesized samples determined by *in situ* XRD and TEM measurements. (1) 1st phase change temperature from amorphous to cubic (rhombohedral); (2) 2nd phase change temperature from cubic (rhombohedral) to primitive trigonal phase

Temperatures determined for	*Via in situ* XRD measurements		*Via in situ* TEM measurements
	1	2	1
$Ge_2Sb_2Te_5$	130 °C	290 °C	132 °C
$Ge_2Sb_2Te_4Se$ (I)	165 °C	270 °C	160 °C
$Ge_2Sb_2Te_2Se_3$ (II)	220 °C	280 °C	222 °C

All established PCMs for optical data storage devices are located in a well-defined area in the map. It seems that the limit of this area for successful optical data storage materials is reached by the values given by the hybridization of $Ge_2Sb_2Te_2Se_3$. This assumption is confirmed by investigations of the optical properties.

The dielectric function ε contains the two dielectric constants ε_1 (real part) and ε_2 (imaginary part).

$$\varepsilon = \varepsilon_1 + i\varepsilon_2 \quad (1)$$

A conversion of the dielectric function leads to the index of refraction n (2) and the extinction coefficient k (3):

$$\varepsilon_1 = n_2 - k_2 \quad (2)$$

$$\varepsilon_2 = 2nk \quad (3)$$

Fig. 7 displays the real and the imaginary part of the dielectric functions of the materials. A significant decrease of the maximum intensity and a shift to higher energies depending on the selenium content is observed. This can be explained by the structural distortions leading to a decrease of resonant bonding, which reduces ε_1 of the crystalline samples of (I) and (II) and explains the behavior.

According to formula (1) and (2) the same trend of the energy dependence of n and k is observed (Fig. 7). For typical amorphous phase change materials the index of refraction is ~50% larger in the crystalline state (*e.g.* $Ge_2Sb_2Te_5$).[15] The substitution of Te by Se leads to a drastic decrease of the difference between the amorphous and crystalline indices of refraction. It is remarkable that the optical constants of the crystalline $Ge_2Sb_2Te_2Se_3$ sample are below amorphous $Ge_2Sb_2Te_5$. This observation implies that the ability of crystalline $Ge_2Sb_2Te_2Se_3$ to reflect light in the appropriate energy range is even worse compared to amorphous $Ge_2Sb_2Te_5$.

Table 4 summarizes the values for the optical constant ε_∞ and the optical bandgap E_g. The values of the amorphous and crystalline phases of $Ge_2Sb_2Te_5$ correspond well with the values reported in literature.[15,62,63]

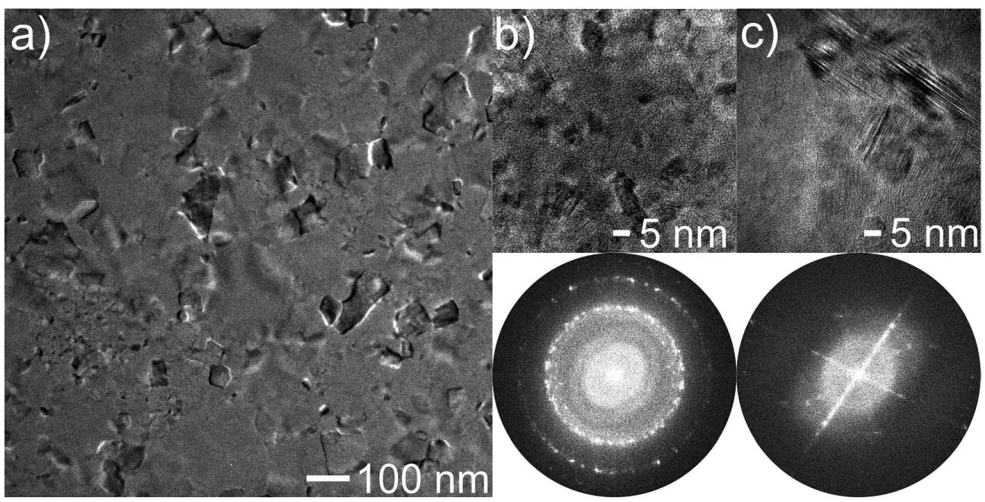

Fig. 4 (a) Bright field image of $Ge_2Sb_2Te_5$. The red and the blue arrow mark a larger grain of about 100 nm and nanocrystals. (b) HRTEM images and corresponding FFT recorded on $Ge_2Sb_2Te_4Se$ and $Ge_2Sb_2Te_2Se_3$ (c) after heating to 150 °C, 190 °C and 250 °C, respectively.

Table 3 Rietveld refinement data of the metastable phase. * = transformed undistorted cell. The cell parameters of the rhombohedral trigonal cell ($R\bar{3}m$) are given according to the hexagonal setting of the space group. Further information is given in Table S4

Chemical formula		225	*	I	II
Space group		$Fm\bar{3}m$ (225)	$R\bar{3}m$ (166)	$R\bar{3}m$ (166)	$R\bar{3}m$ (166)
Cell parameter (Å)	a	6.0251	4.2624	4.1976	4.125
	c	—	10.4408	10.4456	10.4364
c/a			2.4495	2.4885 (+0.0390)	2.5300 (+0.0805)
Crystallite size (nm)		52	—	18	25
R_{Bragg}		1.78	—	1.01	1.92

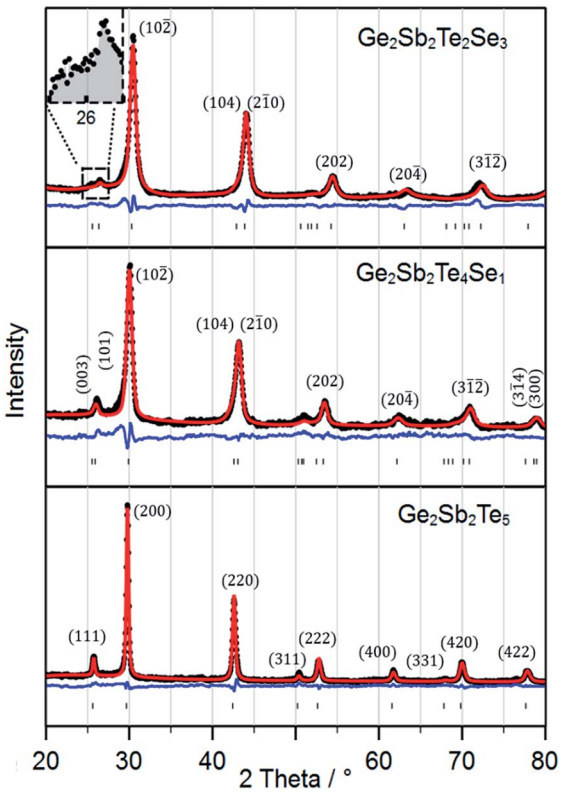

Fig. 5 Powder diffraction pattern of the cubic/rhombohedral trigonal phase after annealing the samples at 180 °C ($Ge_2Sb_2Te_5$), 230 °C (I) and 245 °C (II). Black circles depict the measured data, the red line the refined pattern and the blue line displays the difference of both. Reflection positions are marked by |.

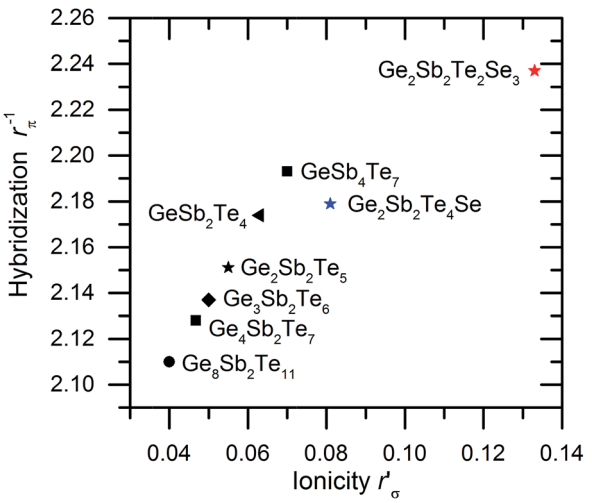

Fig. 6 Calculated values of ionicity and degree of hybridization for some established phase change materials and the substituted compounds.[14] Used radii according to ref. 61.

With increasing selenium content ε_∞ decreases while E_g increases due to the reduced metallic behavior as a result of the substitution of Te by Se. Applying eqn (4) the contribution of resonance bonding can be estimated which is basically the value of the increase of ε_∞ in %.[15]

$$\varepsilon_\infty^{\text{crystalline}}/\varepsilon_\infty^{\text{amorphous}} - 1 \quad (4)$$

The resonance bonding decreases with increasing Se content which can be explained (just like the extraordinary low optical constant of the crystalline phase of (II)) *via* the decrease of resonant bonding in the samples (I) and especially (II). The knowledge of all optical constants allows calculation of the absolute reflectivity of the amorphous and crystalline samples. Fig. 8 displays absolute reflectivity and total contrast calculated according to (5).[42]

$$R_{\text{total}} = \frac{R_{\text{crystalline}} - R_{\text{amorphous}}}{R_{\text{amorphous}}} \quad (5)$$

Due to the pronounced decrease of the absolute reflectivity of the substituted crystalline samples the optical contrast decreases from ~20% for $Ge_2Sb_2Te_5$ to ~17% for (I) and ~8% for (II).

Although a slight shift of the maxima of the dielectric constants to higher energies *e.g.* smaller wavelengths is observed, the Se substituted samples seem to be not suitable for optical phase change data storage. The optical properties confirm the assumption that the limit of the hybridization for materials used in optical data storage devices is reached by values around 2.24.

Sheet resistance measurements

Temperature dependent sheet resistance measurements are shown in Fig. 9. It can be safely assumed that the influence of the slightly different film thicknesses onto resistance data is negligible. The sheet resistances for the amorphous films at room temperature are ~13 MΩ for $Ge_2Sb_2Te_5$, ~73 MΩ for $Ge_2Sb_2Te_4Se$ and ~11 GΩ for $Ge_2Sb_2Te_2Se_3$.

In line with the expected enlargement of the band gap the substitution of Te by Se leads to a giant increase of the sheet resistance of the amorphous phase. The large values of the resistance slightly decrease with increasing temperature until an abrupt drop of 2–4 orders of magnitude is observed at the 1st transition temperatures at about 153 °C for $Ge_2Sb_2Te_5$, 190 °C for (I) and 243 °C for (II). These temperatures correspond well with the temperatures revealed by *in situ* XRD measurements, representing a thoroughly crystallized film (Fig. 2). The electrical contrast between the amorphous and the metastable cubic phase increases significantly from 2 orders of magnitude ($Ge_2Sb_2Te_5$) to 2.5 orders of magnitude (I), and 4 orders of magnitude for (II), referring on the sudden drop of the resistance in Fig. 9. Hence, the electrical contrast of $Ge_2Sb_2Te_2Se_3$ is increased by factor of 100 compared to $Ge_2Sb_2Te_5$. This is an excellent behavior for electrical data storage applications: combining enhanced stability of the amorphous state as well as increasing the readability of the data.

A smooth second drop of the resistivity is caused by the phase change from the cubic into the primitive trigonal phase, which correlates with the slow preformation of the hexagonal

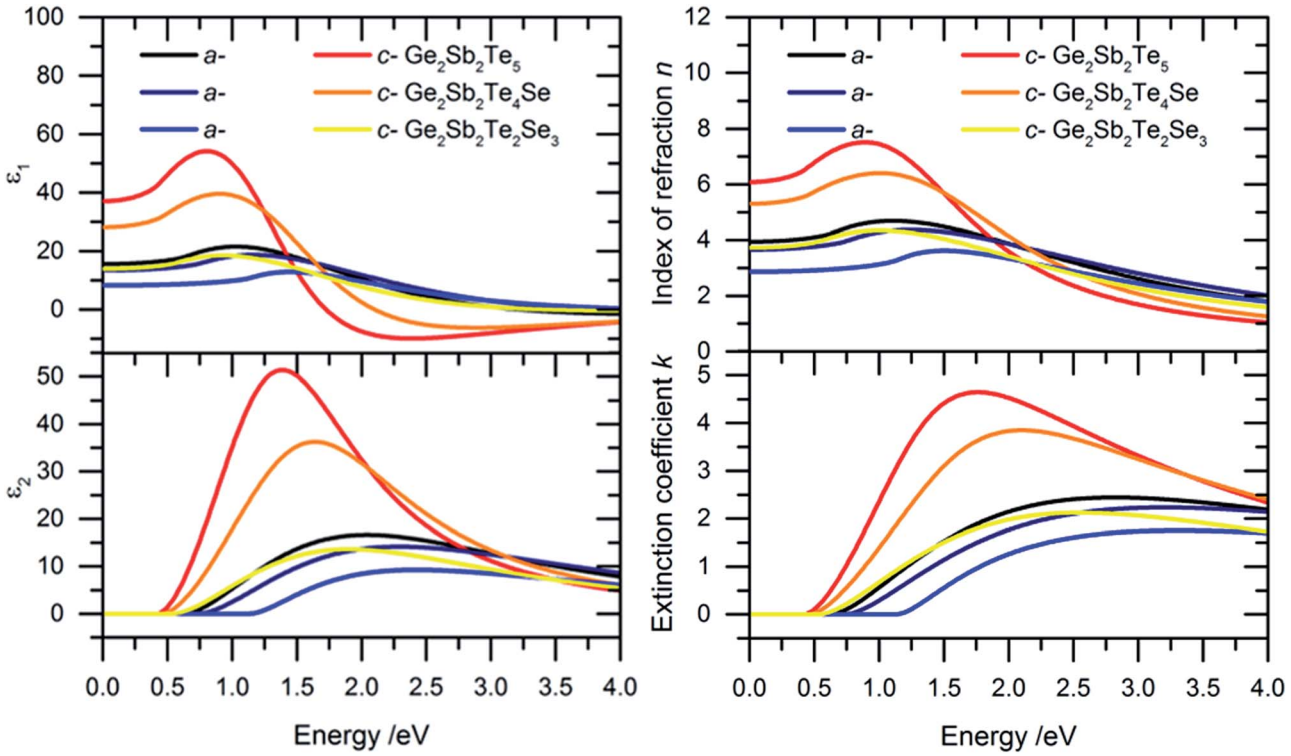

Fig. 7 Left: Dielectric functions ε_1 (top) and ε_2 (bottom) of the amorphous (a-) and crystalline (c-) samples. ε_1 becomes constant for energies below the optical band gap. Functions of ε_2 are depicted without the Drude term. Functions of ε_2 with the Drude term are seen in Fig. S3.† The crystalline samples were annealed at 160 °C (225), 210 °C (I) and 260 °C (II). Right: Index of refraction n (top) and extinction coefficients k (bottom) of the a- and c-samples. k turns out to be zero at energies below the band gaps.

phase observed by the XRD measurements. This phase transition is visible for $Ge_2Sb_2Te_5$ (327 °C) and for (I) at 315 °C, while (II) only shows a slight change in the resistance. Due to the different heating rates the phase change temperatures measured by *in situ* XRD and *in situ* TEM are smaller than the phase change temperatures determined with the sheet resistance measurements. Thus, the second phase change is not complete at 360 °C, which can be seen as the drop in the resistance at 360 °C. This temperature was held constant for 30 min to complete the second phase change. After annealing the resistances remain quite constant at about 25 Ω for $Ge_2Sb_2Te_5$, 40 Ω for (I) and 68 Ω for (II), respectively, which is typical for degenerated semiconductors with high levels of disorder.[64]

Table 4 Dielectric function ε_∞ (degree of polarization) and optical bandgap E_g of the amorphous (a) and crystalline (c) samples. The optical constants were set at energies of 0.05 eV for ε_1 while the Drude contribution was subtracted for the crystalline samples. The optical bandgaps were determined *via* α-10 000 method which is exactly the energy where the absorption reaches 10 000 cm^{-1} (ref. 62)

	Optical constant ε_∞			Optical bandgap E_g		
	a	c	$\%_{increase}$	a	c	$\%_{decrease}$
225	15.6	37.1	138	0.77	0.53	31
I	13.4	28.1	110	0.88	0.59	33
II	8.2	13.9	70	1.23	0.70	43

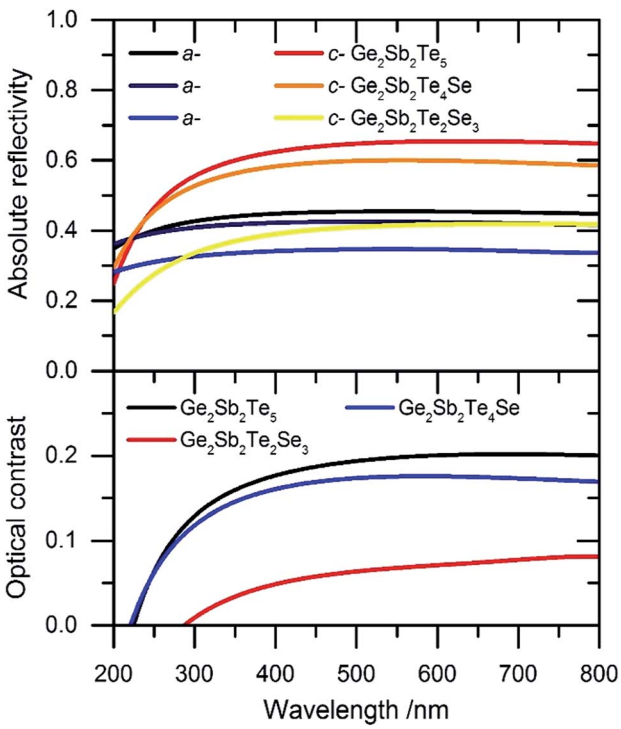

Fig. 8 Calculated absolute reflectivity (top) of the amorphous and crystalline films and total contrast (bottom) of the materials.

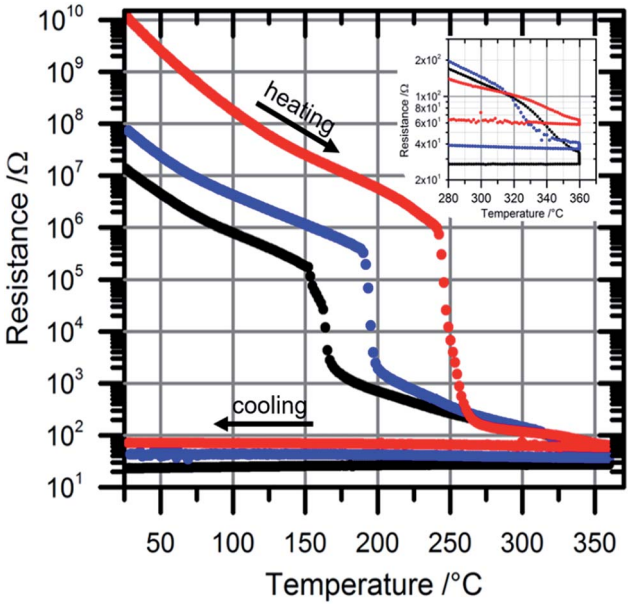

Fig. 9 Sheet resistance measurements of $Ge_2Sb_2Te_5$ (black), $Ge_2Sb_2Te_4Se$ (blue) and $Ge_2Sb_2Te_2Se_3$ (red). The phase change is indicated by a large drop of the sheet resistance. With increasing selenium content the 1st phase change temperature increases as well as the electrical contrast. The 2nd phase change is depicted in the inset.

Conclusion and summary

Two new phase change materials were prepared *via* sputter and physical vapor deposition.

The stability of the amorphous phase and the distortion of the metastable cubic phase significantly increased with increasing selenium content.

The optical constants as well as the optical bandgaps for all the presented materials were determined.

The optical contrast decreased with increasing selenium content due to larger structural distortions in selenium rich crystalline phases and therefore the decrease of resonant bonding. The results suggest that the limit of the area for successful optical data storage materials in the treasure map is reached at high ionicity and hybridization of chemical bonds.

The electrical contrast is significantly improved by selenium substitution and is two orders of magnitudes higher than in the unsubstituted material.

Substitution leads to compositions with exceptional good electrical properties for phase change memory devices at the expense of the optical properties.

Acknowledgements

The authors acknowledge the financial support of the State Schleswig-Holstein. Furthermore, the authors would like to thank David C. Johnson and the Center for Advanced Materials Characterization in Oregon (CAMCOR) for the EPMA measurements and kind support.

References

1 M. Wuttig, *Nat. Mater.*, 2005, **4**, 265–266.
2 W. Bensch and M. Wuttig, *Chem. Unserer Zeit*, 2010, **44**, 92–107.
3 M. Wuttig and N. Yamada, *Nat. Mater.*, 2007, **6**, 824–832.
4 G. W. Burr, M. J. Breitwisch, M. Franceschini, D. Garetto, K. Gopalakrishnan, B. Jackson, B. Kurdi, C. Lam, L. A. Lastras, A. Padilla, B. Rajendran, S. Raoux and R. S. Shenoy, *J. Vac. Sci. Technol., B: Microelectron. Nanometer Struct.–Process., Meas., Phenom.*, 2010, **28**, 223.
5 B.-S. Lee, R. M. Shelby, S. Raoux, C. T. Rettner, G. W. Burr, S. N. Bogle, K. Darmawikarta, S. G. Bishop and J. R. Abelson, *J. Appl. Phys.*, 2014, **115**, 063506.
6 D. Lencer, M. Salinga and M. Wuttig, *Adv. Mater.*, 2011, **23**, 2030–2058.
7 R. Waser, R. Dittmann, M. Salinga and M. Wuttig, *Solid-State Electron.*, 2010, **54**, 830–840.
8 J. Y. Raty, W. Zhang, J. Luckas, C. Chen, R. Mazzarello, C. Bichara and M. Wuttig, *Nat. Commun.*, 2015, **6**, 7467.
9 J. L. F. Da Silva, A. Walsh and H. Lee, *Phys. Rev. B: Condens. Matter Mater. Phys.*, 2008, **78**, 224111.
10 T. Matsunaga, R. Kojima, N. Yamada, K. Kifune, Y. Kubota, Y. Tabata and M. Takata, *Inorg. Chem.*, 2006, **45**, 2235–2241.
11 T. H. Lee and S. R. Elliott, *Phys. Rev. B: Condens. Matter Mater. Phys.*, 2011, **84**, 094124.
12 J. Zhou, Z. Sun, Y. Pan, Z. Song and R. Ahuja, *EPL*, 2011, **95**, 27002.
13 A. V. Kolobov, P. Fons, J. Tominaga and M. Hase, *J. Phys. Chem. C*, 2014, **118**, 10248–10253.
14 D. Lencer, M. Salinga, B. Grabowski, T. Hickel, J. Neugebauer and M. Wuttig, *Nat. Mater.*, 2008, **7**, 972–977.
15 K. Shportko, S. Kremers, M. Woda, D. Lencer, J. Robertson and M. Wuttig, *Nat. Mater.*, 2008, **7**, 653–658.
16 M. Krbal, A. V. Kolobov, P. Fons, J. Tominaga, S. R. Elliott, J. Hegedus and T. Uruga, *Phys. Rev. B: Condens. Matter Mater. Phys.*, 2011, **83**, 054203.
17 M. Krbal, A. V. Kolobov, P. Fons, K. V. Mitrofanov, Y. Tamenori, J. Hegedüs, S. R. Elliott and J. Tominaga, *Appl. Phys. Lett.*, 2013, **102**, 111904.
18 A. V. Kolobov, J. Haines, A. Pradel, M. Ribes, P. Fons, J. Tominaga, Y. Katayama, T. Hammouda and T. Uruga, *Phys. Rev. Lett.*, 2006, **97**, 035701.
19 J. Akola and R. O. Jones, *Phys. Rev. B: Condens. Matter Mater. Phys.*, 2007, **76**, 235201.
20 J. Hegedüs and S. R. Elliott, *Nat. Mater.*, 2008, **7**, 399–405.
21 D. A. Baker, M. A. Paesler, G. Lucovsky, S. C. Agarwal and P. C. Taylor, *Phys. Rev. Lett.*, 2006, **96**, 255501.
22 A. V. Kolobov, P. Fons, J. Tominaga and S. R. Ovshinsky, *Phys. Rev. B: Condens. Matter Mater. Phys.*, 2013, **87**, 165206.
23 C. Lang, S. Ahn Song, D. Nguyen Manh and D. J. H. Cockayne, *Phys. Rev. B: Condens. Matter Mater. Phys.*, 2007, **76**, 054101.
24 S. Kohara, K. Kato, S. Kimura, H. Tanaka, T. Usuki, K. Suzuya, H. Tanaka, Y. Moritomo, T. Matsunaga, N. Yamada, Y. Tanaka, H. Suematsu and M. Takata, *Appl. Phys. Lett.*, 2006, **89**, 201910.

25 J. H. Richter, P. Fons, A. V. Kolobov, S. Ueda, H. Yoshikawa, Y. Yamashita, S. Ishimaru, K. Kobayashi and J. Tominaga, *Appl. Phys. Lett.*, 2014, **104**, 061909.
26 K. V. Mitrofanov, A. V. Kolobov, P. Fons, X. Wang, J. Tominaga, Y. Tamenori, T. Uruga, N. Ciocchini and D. Ielmini, *J. Appl. Phys.*, 2014, **115**, 173501.
27 I. Friedrich, V. Weidenhof, W. Njoroge, P. Franz and M. Wuttig, *J. Appl. Phys.*, 2000, **87**, 4130.
28 V. Weidenhof, I. Friedrich, S. Ziegler and M. Wuttig, *J. Appl. Phys.*, 2001, **89**, 3168.
29 P. Rodenbach, A. Giussani, K. Perumal, M. Hanke, M. Dubslaff, H. Riechert, R. Calarco, M. Burghammer, A. V. Kolobov and P. Fons, *Appl. Phys. Lett.*, 2012, **101**, 061903.
30 N. Yamada and T. Matsunaga, *J. Appl. Phys.*, 2000, **88**, 7020.
31 Y. Sutou, T. Kamada, M. Sumiya, Y. Saito and J. Koike, *Acta Mater.*, 2011, **60**, 872–880.
32 S. Shindo, Y. Sutou, J. Koike, Y. Saito and Y.-H. Song, *Mater. Sci. Semicond. Process.*, 2016, **47**, 1–6.
33 Y. Saito, Y. Sutou and J. Koike, *Appl. Phys. Lett.*, 2013, **102**, 051910.
34 P. Zalden, C. Bichara, J. van Eijk, C. Braun, W. Bensch and M. Wuttig, *J. Appl. Phys.*, 2010, **107**, 104312.
35 G. Bruns, P. Merkelbach, C. Schlockermann, M. Salinga, M. Wuttig, T. D. Happ, J. B. Philipp and M. Kund, *Appl. Phys. Lett.*, 2009, **95**, 043108.
36 M. Putero, M.-V. Coulet, T. Ouled-Khachroum, C. Baehtz and S. Raoux, *APL Mater.*, 2013, **1**, 062101.
37 T. G. Edwards, I. Hung, Z. Gan, B. Kalkan, S. Raoux and S. Sen, *J. Appl. Phys.*, 2013, **114**, 233512.
38 M. Putero, M.-V. Coulet, C. Muller, G. Cohen, M. Hopstaken, C. Baehtz and S. Raoux, *Appl. Phys. Lett.*, 2014, **105**, 181910.
39 M. Putero, M.-V. Coulet, C. Muller, C. Baehtz, S. Raoux and H.-Y. Cheng, *Appl. Phys. Lett.*, 2016, **108**, 101909.
40 J. Tomforde, S. Buller, M. Ried, W. Bensch, D. Wamwangi, M. Heidelmann and M. Wuttig, *Solid State Sci.*, 2009, **11**, 683–687.
41 K. Wang, C. Steimer, D. Wamwangi, S. Ziegler, M. Wuttig, J. Tomforde and W. Bensch, *Microsyst. Technol.*, 2006, **13**, 203–206.
42 S. Buller, C. Koch, W. Bensch, P. Zalden, R. Sittner, S. Kremers, M. Wuttig, U. Schürmann, L. Kienle, T. Leichtweiß, J. Janek and B. Schönborn, *Chem. Mater.*, 2012, **24**, 3582–3590.
43 K. Wang, C. Steimer, D. Wamwangi, S. Ziegler and M. Wuttig, *Appl. Phys. A*, 2005, **80**, 1611–1616.
44 X. Zhou, L. Wu, Z. Song, F. Rao, M. Zhu, C. Peng, D. Yao, S. Song, B. Liu and S. Feng, *Appl. Phys. Lett.*, 2012, **101**, 142104.
45 T. Rosenthal, P. Urban, K. Nimmrich, L. Schenk, J. de Boor, C. Stiewe and O. Oeckler, *Chem. Mater.*, 2014, **26**, 2567–2578.
46 E. M. Vinod, K. Ramesh and K. S. Sangunni, *Sci. Rep.*, 2014, **5**, 8050.
47 E. M. Vinod, K. Ramesh, R. Ganesan and K. S. Sangunni, *Appl. Phys. Lett.*, 2014, **104**, 063505.
48 A. A. Coelho, *TOPAS-Academic. Version 6.0*, 2016.
49 D. Balzar, N. Audebrand, M. R. Daymond, A. Fitch, A. Hewat, J. I. Langford, A. Le Bail, D. Louër, O. Masson, C. N. McCowan, N. C. Popa, P. W. Stephens and B. H. Toby, *J. Appl. Crystallogr.*, 2004, **37**, 911–924.
50 R. W. Cheary and A. A. Coelho, *J. Appl. Crystallogr.*, 1992, **25**, 109–121.
51 W. Theiss, *SCOUT Hard- and Software*.
52 L. J. A. van der Pauw, *Philips Res. Rep.*, 1958, **13**, 1–9.
53 L. J. A. van der Pauw, *Philips Res. Rep.*, 1958, **20**, 220–224.
54 F. M. Smits, *Bell Labs Techn. J.*, 1958, **37**, 711–718.
55 M. A. Green and M. W. Gunn, *Solid-State Electron.*, 1971, **14**, 1167–1177.
56 T. Matsunaga, N. Yamada and Y. Kubota, *Acta Crystallogr.*, 2004, **60**, 685–691.
57 Z. Sun, J. Zhou and R. Ahuja, *Phys. Rev. Lett.*, 2006, **96**, 055507.
58 W. Zhang, A. Thiess, P. Zalden, R. Zeller, P. H. Dederichs, J.-Y. Raty, M. Wuttig, S. Blügel and R. Mazzarello, *Nat. Mater.*, 2012, **11**, 952–956.
59 N. Yamada, E. Ohno, K. Nishiuchi, N. Akahira and M. Takao, *J. Appl. Phys.*, 1991, **69**, 2849.
60 B. J. Kooi, W. M. G. Groot, J. Th and M. De Hosson, *J. Appl. Phys.*, 2004, **95**, 924.
61 J. R. Chelikowsky and J. C. Phillips, *Phys. Rev. B: Condens. Matter Mater. Phys.*, 1978, **17**, 2453.
62 B.-S. Lee, J. R. Abelson, S. G. Bishop, D.-H. Kang, B.-K. Cheong and K.-B. Kim, *J. Appl. Phys.*, 2005, **97**, 093509.
63 T. Kato and K. Tanaka, *Jpn. J. Appl. Phys.*, 2005, **44**, 7340–7344.
64 T. Siegrist, P. Jost, H. Volker, M. Woda, P. Merkelbach, C. Schlockermann and M. Wuttig, *Nat. Mater.*, 2011, **10**, 202–208.

